Journal of Alloys and Compounds 509 (2011) 5023–5027

Contents lists available at ScienceDirect

Journal of Alloys and Compounds

journal homepage: www.elsevier.com/locate/jallcom

Electronic structures and Eu^{3+} photoluminescence behaviors in $Y_2Si_2O_7$ and $La_2Si_2O_7$

Zhiya Zhang[a,b,*], Yuhua Wang[a,b], Feng Zhang[a], Haining Cao[c]

[a] Department of Materials Science, School of Physical Science and Technology, Lanzhou University, Lanzhou, 730000, People's Republic of China
[b] Key Laboratory for Magnetism and Magnetic Materials of the Ministry of Education, Lanzhou University, Lanzhou, 730000, People's Republic of China
[c] Computational Science Center, Korea Institute of Science and Technology, Seoul, 136-791, Republic of Korea

ARTICLE INFO

Article history:
Received 29 November 2010
Received in revised form 5 February 2011
Accepted 7 February 2011
Available online 12 February 2011

PACS:
78.55.−m

Keywords:
$M_2Si_2O_7$: Eu^{3+} (M = Y La)
Electronic band structure
UV–VUV photoluminescence

ABSTRACT

The electronic structures and linear optical properties of $Y_2Si_2O_7$ (YSO) and $La_2Si_2O_7$ (LSO) are calculated by LDA method based on the theory of DFT. Both YSO and LSO are direct-gap materials with the direct band gap of 5.89 and 6.06 eV, respectively. The calculated total and partial density of states indicate that in both YSO and LSO the valence band (VB) is mainly constructed from O 2p and the conduction band (CB) is mostly formed from Y 4d or La 5d. Both the calculated VB and CB of YSO exhibit relatively wider dispersion than that of LSO. In addition, the CB of YSO presents more electronic states. Meanwhile, the VB of LSO shows narrower energy distribution with higher electronic states density. The theoretical absorption of YSO shows larger bandwidth and higher intensity than that of LSO. The results are compared with the experimental host excitations and impurity photoluminescence in Eu^{3+}-doped YSO and LSO.

1. Introduction

The success in developing vacuum violet (VUV) light sources from rare-gas plasma and excimer discharges has realized the applications of VUV phosphors in Hg-free lamps, plasma display panels (PDPs), liquid crystal display (LCD) backlights [1–6] and other optoelectronic fields [7,8]. However, current VUV phosphors do not have sufficient conversion efficiency due to high energy losses during the nonradiative relaxation process. The efficiency of VUV phosphors, such as those used in PDP display, is very low (1–1.5 lm/W), compared with fluorescent lamps (80–100 lm/W) and cathode-ray tubes (CRTs) (5–6 lm/W). In addition, there are some other fatal drawbacks such as poor color purity for the commercial red phosphor (Gd, Y)BO_3:Eu^{3+}, too long decay time for the green Zn_2SiO_4:Mn^{2+} and low degradation stability for the blue $BaMgAl_{10}O_{17}$:Eu^{2+} [9–11]. In order to solve these problems, considerable research activities such as empirical doping, morphology modification, fabrication process improving as well as new phosphors exploring [12–18] have been made during the past few years. Despite all these efforts, the premium solution to the major problems mentioned above is to develop a better understanding of the VUV photoluminescence (PL) mechnisms. For VUV phosphors, the absorption of VUV photons takes place either in luminescent centers or in host lattice. In the former case, the VUV photons excite directly the luminescent centers and then produce visible light. Instead, the excitation in host lattice, i.e. host excitation, is indirect and the excitation energy is firstly transferred to the luminescent centers, which emit visible light subsequently. In host excitation, which in most cases dominates the VUV excitation process, the electronic transitions from the valence band (VB) to the conduction band (CB) are always involved. Usually, the transition probability depends sensitively on the nature of the VB and CB states. Therefore, a good understanding of the electronic states near the band gap or in the absorption edge region between 6 and 8 eV in large gap materials is essential for studying the VUV PL behaviors and designing new efficient VUV phosphors. Great efforts have been dedicated to demonstrate the correlation between the nature of the electronic properties and the PL performance of phosphors [19–21].

$Y_2Si_2O_7$ and $La_2Si_2O_7$ are two important disilicates. Y-type $Y_2Si_2O_7$ (YSO) and G-type $La_2Si_2O_7$ (LSO) are monoclinic with the space group (SG) of $P121/a1$ (SG No. 14) (ICSD #28212) [22] and $P121/c1$ (SG No. 14) (ICSD #74775) [23], respectively. As early in 1969, Ce^{3+} doped YSO was reported as a high efficient cathode-ray (CR) phosphors with short decay time [24]. The UV PL properties of YSO doped with rare-earth ions were investigated in recent literatures [25–27]. In our previous study [28], we doped YSO and LSO

* Corresponding author at: School of Physical Science and Technology, Lanzhou University, Lanzhou, 730000, People's Republic of China. Tel.: +86 931 8912772; fax: +86 931 8913554.
E-mail address: zhangzhiya@lzu.edu.cn (Z. Zhang).

0925-8388/$ – see front matter © 2011 Elsevier B.V. All rights reserved.
doi:10.1016/j.jallcom.2011.02.039

with 5% Eu^{3+} which act as the luminescent centers and studied their UV and VUV PL properties. It was found that $Y_2Si_2O_7$:Eu^{3+} (YSOE) exhibited much lower PL intensity in UV region while much higher PL intensity in VUV region when compared with $La_2Si_2O_7$:Eu^{3+} (LSOE). The ionic size of Eu^{3+} is smaller than that of La^{3+} and slightly larger than that of Y^{3+}. In the same coordination environment, the radius difference is estimated to be about 8% between Eu^{3+} and La^{3+} and about 5% between Eu^{3+} and Y^{3+}. Even when the radius of La^{3+} is 15% larger than that of Y^{3+}, Monteverde and co-workers [29,30] found that Y^{3+} in YSO can be completely replaced by La^{3+} accompanied by a deformation of [SiO_4] tetrahedral. In our work, only a fraction of 5% of the total Y^{3+} (in YSO) or La^{3+} (in LSO) sites are expected to be replaced by Eu^{3+}. Even if a slightly different solid solubility of Eu^{3+} in YSOE and LSOE occurs with respect to the above discussed radius differences, it may not result in the opposite UV–VUV PL properties in the two phosphors. Another consideration is that the substitution defects would be higher in LSOE due to the larger radius difference between Eu^{3+} and La^{3+}. But the defects would just cut down both the UV and VUV PL intensity rather than leading to the observed opposite UV–VUV PL properties.

In the present work we perform a theoretical calculation of density functional theory (DFT) with the local density approximation (LDA) on the two hosts of YSO and LSO, and explore how Y ([Kr] $4d^15s^2$) and La ([Xe] $5d^16s^2$) contribute to the corresponding host lattice electronic structures and influence the impurity (Eu^{3+}) PL properties.

2. Experimental and computational details

The quantum efficiency of phosphors is the ratio of the output (excitation or emission) to the input (absorption) of the photons. The quantum efficiency of YSOE and LSOE in UV region are determined by collecting all the absorbed and emitted photons using an integrating sphere with the HORIBA JOBIN YVON Fluorlog-3 spectrofluorometer system (Edison, NJ).

LDA approximation within DFT [31,32] is used throughout this work. CASTEP [33,34] employed in the present work is based on plane-waves and pseudopotentials. The wave functions describe only the valence and the conduction electrons, and the core electrons are taken into account using pseudopotentials. The preconditioned conjugate gradient (CG) band-by-band method [35] and the Pulay density mixing scheme [34] are used throughout the calculation to guarantee an efficient locating of the energy minimum of the electronic ground state. Also, the optimized pseudopotential in the Kleinman–Bylander form [36–38] provides a small plane-wave basis set and simultaneously meets the accuracy required by our current study. The Read and Needs correction [39] is applied to ensure accurate optical matrix elements calculations in non-local-pseudopotential-based method. The configurations of YSO and LSO employed in the present calculations are from literatures [22] and [23], respectively. The lattice parameters of YSO (a = 5.54 Å, b = 10.78 Å, c = 4.66 Å, β = 96.1°) [22] and LSO (a = 5.4109 Å, b = 8.7976 Å, c = 14.287 Å, β = 112.74°) [23] used in the calculation are similar to these of our prepared samples [28]. Before the total energy calculations, geometry optimizations are performed in order to obtain an accurate bulk modulus. The considered valence electrons for Y, La, Si and O are $4d^15s^2$, $5d^16s^2$, $3s^23p^2$ and $2s^22p^4$, respectively. A kinetic-energy cutoff of 450 eV and a self-consistent field (SCF) tolerance threshold of 2.0×10^{-6} eV/atom were used for both YSO and LSO. Based on the calculated band structure, a scissors operator [40] is introduced and the linear optical properties of YSO and LSO crystals are evaluated.

3. Results and discussion

The calculated band structure of YSO and LSO are shown in Fig. 1. YSO and LSO both are direct-gap materials. The direct band gap (E_g) are presented to be 5.89 and 6.06 eV, respectively. Ching and his colleagues calculated the electronic and optical properties of Y_2SiO_5 and $Y_2Si_2O_7$ with comparisons to α-SiO_2 and Y_2O_3 [41]. In their work, they employed the *ab initio* orthogonalized linear combination of atomic orbitals (OLCAO) method and obtained the direct gap of $Y_2Si_2O_7$ as 4.78 eV. The experimentally determined E_g was reported to be 6.9 eV using a diffuse reflectivity spectrum method by Mayolet and Krupa [42]. We can see that the calculated E_g in both Ching's and our work are smaller than the experimental result. This error is common and inherent for LDA method due to the discontinuity of exchange-correlation energy [43]. In Fig. 1, the VB of LSO

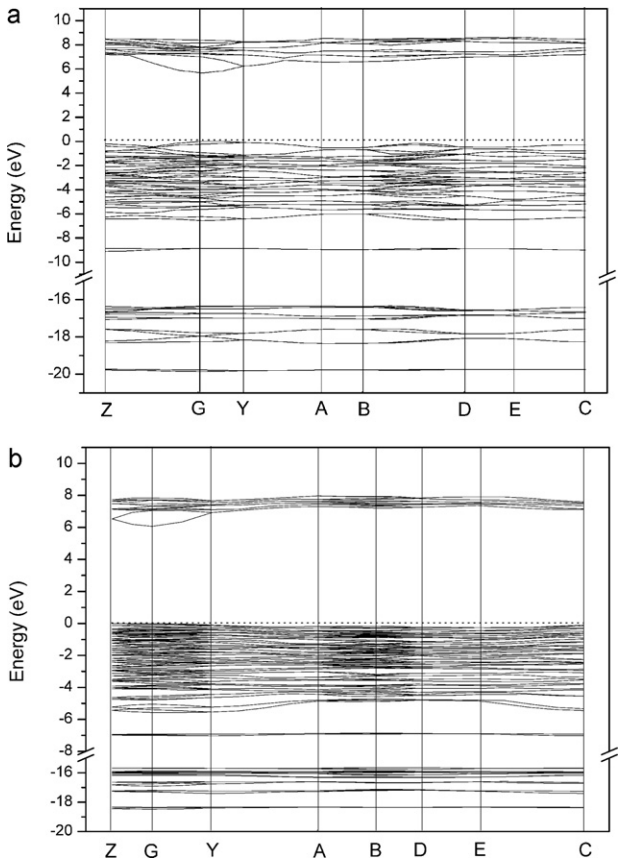

Fig. 1. Calculated band structures of (a) YSO and (b) LSO crystals.

is very flat while that of YSO fluctuates obviously. Both the VB and CB of YSO exhibit relatively wider dispersion. By comparison, the VB of LSO is more compressed with narrower energy distribution and higher states density, and in addition, the CB of LSO exhibits decreased total number of electronic states.

Figs. 2 and 3 present the calculated total density of states (DOS) and partial density of states (PDOS). Each curve can be divided into three regions. For YSO, the lowest states at about −17 eV (bandwidth (B.W.) = 5.35 eV) are projected to be O 2s (major), Si 3s and 3p (minor) and Y (minor) orbits. The states around −4 eV (B.W. = 8.98 eV) are mainly composed of O 2p orbits forming the VB of YSO. Additionally, Si 3p and 3s orbits hybridize with the O 2p orbits and contribute to the VB. Also, a fraction of the Y orbits are involved in the VB. The CB of YSO is around 5 eV (B.W. = 4.38 eV) comprising Y 4d (major) and Si (minor) orbits. As for LSO, the lowest states around −17 eV including O 2s (major), Si (minor) and Y (minor) orbits present the B.W. of 3.62 eV. The VB at −4 eV with a B.W. of 6.94 eV comprises O 2p orbits (major), also Si and La orbits (minor). The CB of LSO is located around 6 eV with a B.W. of 3.19 eV and includes La 5d (major) and Si (minor) orbits. From the plots in Figs. 2 and 3 discussed above, we can conclude that: (1) in YSO and LSO, the Si–O bond is mainly covalent and the (Y/La)–O bond is mainly ionic in nature; (2) both VB and CB states of YSO are more dispersed in k-space than those of LSO; (3) the VB top of LSO presents much steeper edge; (4) the CB (Y 4d) of YSO present apparently wider DOS distribution and larger total electronic states number than that (La 5d) of LSO. These results consist well with the band structures of YSO and LSO discussed previously in Fig. 1.

Based on the calculated band structures, the theoretical absorption curves for YSO and LSO are obtained in Fig. 4. As can be seen, the absorption of YSO features larger bandwidth and higher intensity when compared with that of LSO. Fig. 5 exhibits the experimen-

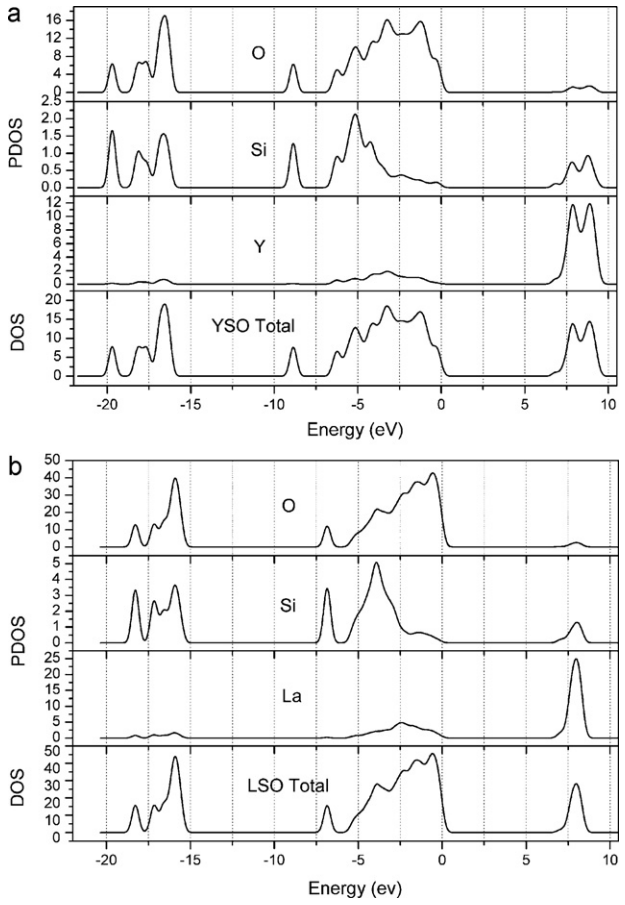

Fig. 2. Total DOS and projected PDOS of (a) YSO and (b) LSO crystals.

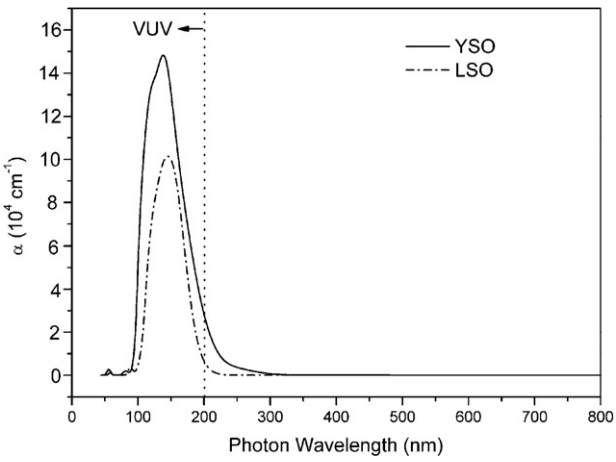

Fig. 4. Theoretical absorption curves for YSO (solid) and LSO (dash dot) crystals.

tal UV–VUV excitation spectra of YSOE and LSOE [28]. It is obvious that the excitation of YSOE in VUV region ($\lambda < 200$ nm) is stronger than that of LSOE while that in UV region ($\lambda > 200$ nm) shows the opposite trend. As stated previously, E_g of YSO has been experimentally determined to be 6.9 eV (~180 nm) [42], which corresponds to the optical absorption edge of YSO. In Fig. 5, the excitations in VUV region, which can be primarily assigned to the host excitation, also start from about 180–190 nm. As previously concluded from Figs. 1–3, in YSO, the VB states are more dispersed and the CB exhibit more electronic states and wider energy distribution. So, the electrons in YSO VB are more delocalized and tend to be excited with high probability, meanwhile, YSO CB is expected to capture the excited electrons and then transfer the energy to the luminescent centers more efficiently. In addition, due to the smaller radius difference between Eu^{3+} and Y^{3+}, YSOE has less substitution defects, which weaken the energy transfer between the host and the luminescent center. So, YSOE is supposed to have relatively higher energy transfer efficiency than LSOE. Because the excitation

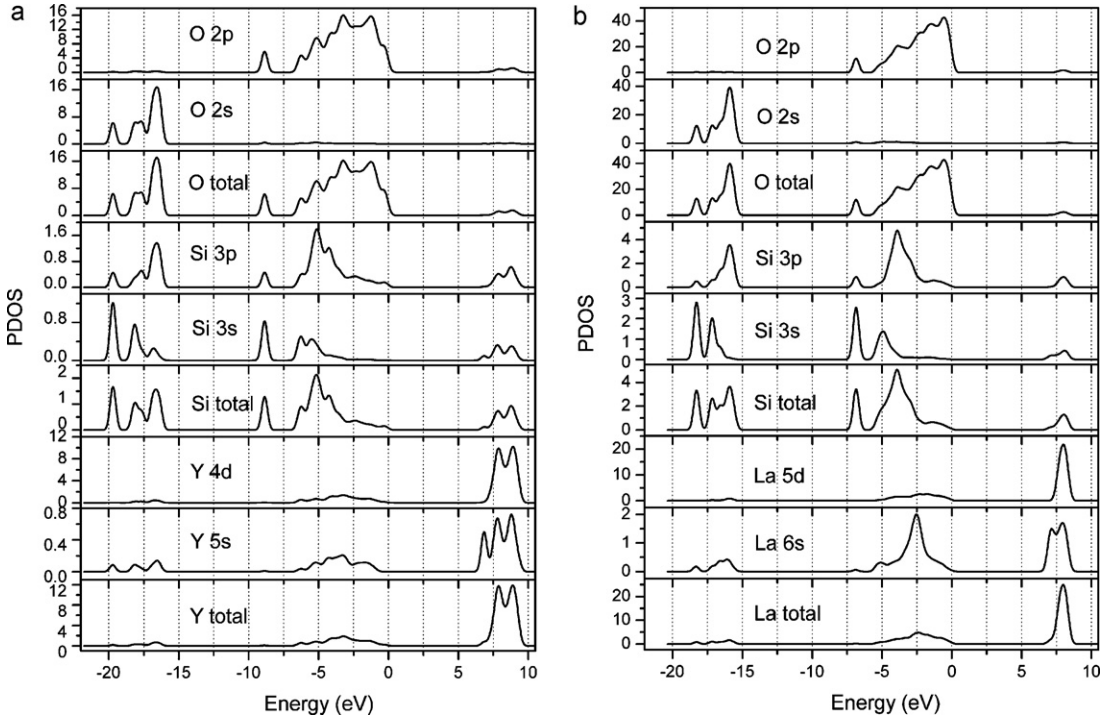

Fig. 3. Orbit-resolved PDOS of (a) YSO and (b) LSO crystals.

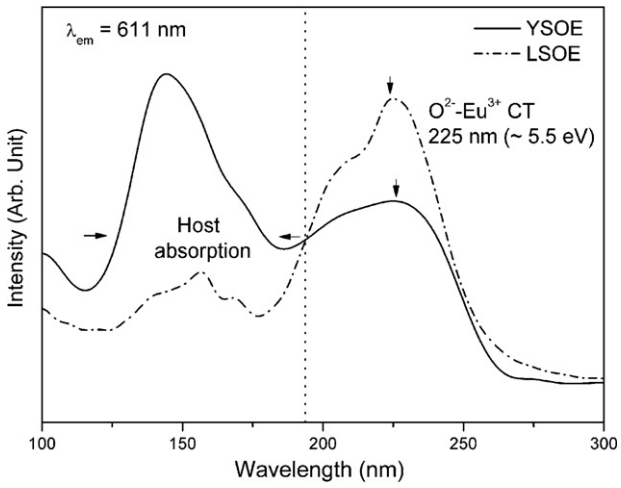

Fig. 5. Experimental UV and VUV excitation spectra of YSOE (solid) and LSOE (dash dot) (monitor = 611 nm).

efficiency is the product of the absorption efficiency and the energy transfer efficiency, YSOE should present a stronger excitation in VUV region than LSOE, which agrees well with the experimental results implied in Fig. 5.

In Fig. 5, the excitations in UV region are due to O^{2-}–Eu^{3+} charge transfer (CT) transitions. The O^{2-}–Eu^{3+} CT energy is presented to be about 225 nm (~5.5 eV) for YSOE and LSOE. This value is similar to the reported 5.56 eV for Eu^{3+} doped YSO [44]. As can be seen, the O^{2-}–Eu^{3+} CT intensity is much higher in LSOE. As stated earlier in this work, the result cannot be interpreted by the radius difference between Y^{3+} and La^{3+}. According to Li et al. [45], O^{2-}–Eu^{3+} CT can be viewed as the electronic transition that starts from the top of VB and ends up at the Eu^{2+} ground state. From this point of view, the electronic states near the top of VB would be especially crucial to the O^{2-}–Eu^{3+} CT. Fig. 6(a) and (b) shows the DOS distribution near the VB top (−4 to 0 eV) and the O^{2-}–Eu^{3+} CT scheme for YSOE and LSOE. It is obvious that there are more electronic states near the top VB of LSO. Accordingly, when the electrons are transferred from the VB top to the Eu^{2+} ground state in LSOE, there would be more electronic states being involved and LSOE correspondingly should have higher probability of UV photons absorption. Meanwhile, the quantum efficiency of YSOE and LSOE are determined to be 75.8% and 73.3%, respectively, with 254 nm excitation at room temperature. Even though the quantum efficiency is similar for YSOE and LSOE, the much higher UV excitation of LSOE can be observed due to its more intensive absorption probability of UV light. In Fig. 6, we assume that the Eu^{2+} levels are the same in YSO and LSO with respect to the similar O^{2-}–Eu^{3+} CT positions in YSOE and LSOE observed in Fig. 5.

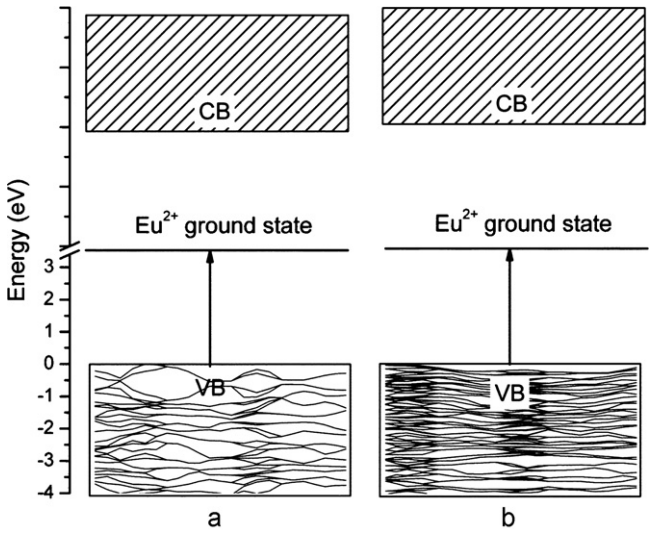

Fig. 6. The electronic states distribution near the host VB top and the O^{2-}–Eu^{3+} CT scheme in (a) YSOE and (b) LSOE.

4. Conclusions

The contributions of subsystems to the host band structures and optical responses of YSOE and LSOE are analyzed using plane-wave pseudo-potential method based on the DFT and LDA theory. YSO and LSO are presented as direct-gap materials with the direct band gap of 5.89 eV and 6.06 eV, respectively. The VB of the two crystals is mainly constructed from O 2p states and the CB is mostly formed from Y 4d or La 5d states. In the two crystals, Si–O bond is mainly covalent and (Y/La)–O bond is dominantly ionic in nature. In YSO, both the VB and CB possess more dispersed electronic states distribution and the CB presents increased total number of electronic states. The VB top of LSO shows steeper edge with more compressed energy distribution and higher states density. The theoretical absorption in YSO features larger bandwidth and higher intensity when compared with that in LSO. These results well explain why YSOE exhibited stronger host excitation while lower O^{2-}–Eu^{3+} CT intensity than LSOE.

Acknowledgements

This work is supported by the Youth Innovation Research Fund for Interdisciplince of Lanzhou University (LZUJC200906) and National Science Foundation for Distinguished Young Scholars (50925206).

References

[1] X.X.Z.C Li, Y.H. Wang, J. Alloys Compd. 472 (2009) 521.
[2] J.H. Lee, M.H. Heo, S.-J. Kim, S. Nahm, K. Park, J. Alloys Compd. 473 (2009) 272.
[3] M. Xie, H. Liang, Q. Su, Y. Huang, Z. Gao, Y. Tao, Electrochem. Solid-State Lett. 13 (2010) J140.
[4] Q. Dong, Y. Wang, Z. Wang, X. Yu, B. Liu, J. Phys. Chem. C 114 (2010) 9245.
[5] D. Wang, N. Kodama, L. Zhao, Y. Wang, J. Electrochem. Soc. 157 (2010) J233.
[6] Z. Wang, Y. Wang, Y. Li, B. Liu, J. Alloys Compd. 509 (2011) 343.
[7] G. Dominiak-Dzik, W. Ryba-Romanowski, L. Kovacs, E. Beregi, Radiat. Meas. 38 (2004) 557.
[8] J. Andrzej, Wojtowicz, Opt. Mater. 31 (2009) 474.
[9] K.Y. Jung, Physica B: Condens. Mater. 405 (2010) 3195.
[10] J. Liu, Y. Wang, X. Yu, J. Li, J. Lumin. 130 (2010) 2171.
[11] Z.H. Zhang, Y.H. Wang, X.X. Li, J. Alloys Compd. 478 (2009) 801.
[12] Y. Wang, L. Wang, Mater. Lett. 60 (2006) 2645.
[13] J.H. Seo, S.H. Sohn, Mater. Lett. 64 (2010) 1264.
[14] P. Zhu, W. Di, Q. Zhu, B. Chen, H. Zhu, H. Zhao, Y. Yang, X. Wang, J Alloys Compd. 454 (2008) 245.
[15] Y.F. Wang, X. Xu, L.J. Yin, L.Y. Hao, J. Am. Ceram. Soc. 93 (2010) 1534.
[16] J. Zhang, Y. Wang, Z. Zhang, X. Peng, Y. Jiang, H. Li, Mater. Res. Bull. 44 (2009) 953.
[17] V. Sivakumar, G.Y. Hong, J.S. Kim, D.Y. Jeon, J. Lumin. 129 (2009) 1632.
[18] A.R. Lakshmanan, S.-B. Kim, H.M. Jang, B.G. Kum, B.K. Kang, S. Heo, D. Seo, Adv. Funct. Mater. 17 (2007) 212.
[19] Y. Wang, Z. Zhang, J. Zhang, Y. Lu, J. Solid State Chem. 182 (2009) 813.
[20] F. Zhang, Y. Wang, Z. Zhang, B. Liu, J. Mater. Res. 25 (2010) 842.
[21] J. Andrzej, Wojtowicz, Opt. Mater. 31 (2009) 1772.
[22] N.G. Batalieva, Y.A. Pyatenko, J. Struct. Chem. 9 (1968) 921.
[23] A.N.Z Christensen, Kristallogr 209 (1994) 7.
[24] A.H. Gomes de Mesquita, A. Bril, Mater. Res. Bull. 4 (1969) 643.
[25] Q.Y. Zhang, K. Pita, W. Ye, W.X. Que, C.H. Kam, Chem. Phys. Lett. 356 (2002) 161.
[26] P. Zhou, X. Yu, L. Yang, S. Yang, W. Gao, J. Lumin. 124 (2007) 241.
[27] H. Yang, Y. Liu, S. Ye, J. Qiu, Chem. Phys. Lett. 451 (2008) 218.
[28] Z. Zhang, Y. Wang, Mat. Res. Soc. Symp. Proc. 916 (2006) 35.
[29] F. Monteverde, G. Celotti, J. Eur. Ceram. Soc. 22 (2002) 721.
[30] F. Monteverde, G. Celotti, J. Eur. Ceram. Soc. 19 (1999) 2021.
[31] P. Hohenberg, W. Kohn, Phys. Rev. 136 (1964) B864.
[32] W. Kohn, L.J. Sham, Phys. Rev. 140 (1965) A1133.
[33] CASTEP 3.5 program developed by Molecular Simulations Inc., 1997.

[34] M.C. Payne, M.P. Teter, D.C. Allan, T.A. Arias, J.D. Joannopoulos, Rev. Mod. Phys. 64 (1992) 1045.
[35] G. Kresse, J. Furthmüller, Phys. Rev. B 54 (1996) 11169.
[36] A.M. Rappe, K.M. Rabe, E. Kaxiras, J.D. Joannopoulos, Phys. Rev. B 41 (1990) 1227.
[37] J.S. Lin, A. Qteish, M.C. Payne, V. Heine, Phys. Rev. B 47 (1993) 4174.
[38] L. Kleinman, D.M. Bylander, Phys. Rev. Lett. 48 (1982) 1425.
[39] A.J. Read, NeedsF R. J., Phys. Rev. B 44 (1991) 13071.
[40] R.W. Godby, M. Schluter, L.J. Sham, Phys. Rev. B 37 (1988) 10159.
[41] W.Y. Ching, L. Ouyang, Y.-N. Xu, Phys. Rev. B 67 (2003) 245108.
[42] A. Mayolet, J.C. Krupa, J. Soc. Inf. Display 4 (1996) 173.
[43] D.I. Thomson, Doctoral Dissertation, University of Cambrige, 1997.
[44] P. Dorenbos, J. Lumin. 111 (2005) 89.
[45] L. Li, S. Zhang, J. Phys. Chem. B 110 (2006) 21438.